SECOND EDITION

Nucleosynthesis and Chemical Evolution of Galaxies

Bernard E. J. Pagel

CAMBRIDGE

CAMBRIDGE www.cambridge.org/9780521840309

This page intentionally left blank

NUCLEOSYNTHESIS AND CHEMICAL EVOLUTION OF GALAXIES

Second Edition

The distribution of elements in the cosmos is the result of many processes, and it provides a powerful tool to study the Big Bang, the density of baryonic matter, nucleosynthesis and the formation and evolution of stars and galaxies. This textbook, by a pioneer of the field, provides a lucid and wide-ranging introduction to the interdisciplinary subject of galactic chemical evolution for advanced undergraduates and graduate students. It is also an authoritative overview for researchers and professional scientists.

In this textbook many exciting topics in astrophysics and cosmology are covered, from abundance measurements in astronomical sources, to light element production by cosmic rays and the effects of galactic processes on the evolution of the elements. Simple derivations for key results are provided, together with problems and helpful solution hints, enabling the student to develop an understanding of results from numerical models and real observations.

This new edition includes results from recent space missions, including WMAP and FUSE, new material on abundances from stellar populations, nebular analysis and meteoric isotopic anomalies, and abundance analysis of X-ray gas, and several extra problems at the end of chapters.

NUCLEOSYNTHESIS AND CHEMICAL EVOLUTION OF GALAXIES

Second Edition

BERNARD PAGEL

Visiting Professor of Astronomy
University of Sussex
Emeritus Professor of Astrophysics at NORDITA
Copenhagen

CAMBRIDGE
UNIVERSITY PRESS

CAMBRIDGE UNIVERSITY PRESS
Cambridge, New York, Melbourne, Madrid, Cape Town, Singapore, São Paulo

Cambridge University Press
The Edinburgh Building, Cambridge CB2 8RU, UK
Published in the United States of America by Cambridge University Press, New York

www.cambridge.org
Information on this title: www.cambridge.org/9780521840309

First published in print format 2009

ISBN-13 978-0-511-50075-6 eBook (Adobe Reader)

ISBN-13 978-0-521-84030-9 hardback

Bernard E. J. Pagel

Bernard Ephraim Julius Pagel was born in Berlin on 4 January 1930, but when his father was dismissed from his post as Jewish persecution increased, the family moved to Britain in 1933. From Merchant Taylors' School he won an open scholarship in Natural Sciences at Sidney Sussex College, Cambridge, graduating with First-class honours in Physics in 1950. His early research at Cambridge (Ph.D. 1955) centred on the solar atmosphere. Inspired by Willy Fowler, a future Nobel Prize winner who was visiting from California, he started a life-long interest in the abundances of the chemical elements.

In 1956 he moved to the Royal Greenwich Observatory at Herstmonceux Castle, Sussex. A search for more accurate estimates of chemical abundances led him to develop new analytic methods of analyzing the spectra of stars. By 1967, Sussex University had established an M.Sc. programme in astronomy, where Bernard lectured. During the early 1970s he began to develop the simple but elegant theoretical models to describe the chemical evolution of galaxies that have served as a foundation for the subject.

In 1975, using the new Anglo-Australian Telescope, Bernard started a long series of collaborations on the abundance analysis of H II regions in external galaxies, starting with the Magellanic Clouds. This led to the development of a method of estimating rough values for chemical abundances when observational data were sparse and only the strongest lines could be seen. Despite the method's acknowledged limitations, it had enormous influence as modern detectors allowed spectroscopic observation of faint galaxies. Variants of the method are still extensively used today. Further collaboration through observatories in the Canary Islands resulted in his fruitful influence on a generation of Spanish research students.

Retirement at 60 from his happy years at Herstmonceux was compulsory, so he moved in 1990 to a Chair at the Nordic Institute for Theoretical Astrophysics in Copenhagen. He became respected throughout Scandinavian astronomy, aided by his extraordinary facility for languages. A major programme was completed on the determination of the primordial helium abundance, and he started new joint work on the chemical evolution of our own Galaxy. By the time he had 'retired' again in 1998, this time from Copenhagen back to Sussex, he had written the first edition of *Nucleosynthesis and Chemical Evolution of Galaxies*, the revisions for the second edition of which he had virtually completed just before his death on 14 July 2007.

He could be a formidable, but always fair, critic, and gave freely of his time to those who asked for help and advice. The Pagel family household in Ringmer, Sussex, will be warmly remembered by many visiting astronomers. Bernard loved classical music – often playing the piano with great enthusiasm, if not with quite the accuracy of his abundance determinations! He will be remembered with great affection, particularly for the beady-eyed look over his pipe and a quick and brilliant intelligence which would even put one of his heroes, Sherlock Holmes, to shame.

To Annabel

Contents

List of abbreviations

A & A	*Astronomy & Astrophysics*
ABB	after the Big Bang
AGB	asymptotic giant branch
AGN	active galactic nucleus
AMR	age–metallicity relation
amu	atomic mass unit
Ap. J.	*Astrophysical Journal*
AQ	Astrophysical Quantities, by C. W. Allen
Astr. J.	*Astronomical Journal*
B^2FH	E. M. and G. R. Burbidge, Fowler and Hoyle
BABI	basaltic achondrite
BBNS	Big Bang nucleosynthesis
BCG	blue compact galaxy
BDM	baryonic dark matter
B.E.	binding energy
BSG	blue supergiant
CAI	calcium-aluminium-rich inclusion
CC1	carbonaceous chondrite type 1
CDM	cold dark matter
CERN	European Council for Nuclear Research (Geneva)
CM	centre of mass
CNO	carbon, nitrogen and oxygen
CO	CO molecule, or carbon and oxygen
CP	chemically peculiar
DDO	David Dunlap Observatory, Toronto, intermediate-band system
2DF	two-degree field
3DHO	three-dimensional harmonic oscillator
E-AGB	early AGB

ELS	Eggen, Lynden-Bell and Sandage
EW	equivalent width
FIP	first ionization potential
FUN	fractionation and unknown nuclear
FUSE	Far Ultraviolet Spectroscopic Explorer
GCE	Galactic chemical evolution
GCR	Galactic cosmic ray
GT	Gamow–Teller
GUT	grand unification theory
HB	horizontal branch
HR	Hertzsprung–Russell
HST	Hubble Space Telescope
IGM	intergalactic medium
IMF	initial mass function
IMS	intermediate-mass stars
IR	infrared
IRAS	Infra-Red Astronomy Satellite
ISM	interstellar medium
ISW	infinite square well
IUE	International Ultraviolet Explorer
KBH	Kulkarni, Blitz and Heiles
K.E.	kinetic energy
LBG	Lyman-break galaxy
LEP	Large Electron–Positron Collider
LINER	low-ionization nuclear emission line region
LMC	Large Magellanic Cloud
LTE	local thermodynamic equilibrium
MEMMU	Milne, Eddington, Minnaert, Menzel and Unsöld
MNRAS	*Monthly Notices of the Royal Astronomical Society*
MS	main sequence
MWB	microwave background radiation
NDM	non-baryonic dark matter
ORS	Oliver, Rowan-Robinson and Saunders
PDMF	present-day mass function
PN	planetary nebula
PP	Partridge and Peebles
QM	quantum mechanics
QSO	quasi-stellar object
RGB	red-giant branch
RSG	red supergiant

SBBN	standard Big Bang nucleosynthesis
SDSS	Sloan Digital Sky Survey
SFR	star formation rate
SGB	subgiant branch
SMC	Small Magellanic Cloud
SN	supernova
SN Ia	Type Ia supernova
SN II	Type II supernova
SNR	supernova remnant
snu	solar neutrino unit
SSP	single stellar population
SZ	Searle and Zinn
TAMS	terminal main sequence
TP-AGB	thermal pulse AGB
UBV	Johnson UBV broad-band system
UV	ultraviolet
WMAP	Wilkinson Microwave Anisotropy Probe
WIMPS	weakly interacting massive particles
WR	Wolf–Rayet
ZAHB	zero-age horizontal branch
ZAMS	zero-age main sequence

Preface to the first edition

This book is based on a lecture course given at Copenhagen University in the past few years to a mixed audience of advanced undergraduates, graduate students and some senior colleagues with backgrounds in either physics or astronomy. It is intended to cover a wide range of interconnected topics including thermonuclear reactions, cosmic abundances, primordial synthesis of elements in the Big Bang, stellar evolution and nucleosynthesis. There is also a (mainly analytical) treatment of factors governing the distribution of element abundances in stars, gas clouds and galaxies and related observational data are presented.

Some of the content of the course is a concise summary of fairly standard material concerning abundance determinations in stars, cold gas and ionized nebulae, cosmology, stellar evolution and nucleosynthesis that is available in much more detail elsewhere, notably in the books cited in the reading list or in review articles; here I have attempted to concentrate on giving up-to-date information, often in graphical form, and to give the simplest possible derivations of well-known results (e.g. exponential distribution of exposures in the main s-process). The section on Chemical Evolution of Galaxies deals with a rapidly growing subject in a more distinctive way, based on work in which I and some colleagues have been engaged over the years. The problem in this field is that uncertainties arising from problems in stellar and galactic evolution are compounded. Observational results are accumulating at a rapid rate and numerical models making a variety of often arbitrary assumptions are proliferating, leading to a jungle of more or less justifiable inferences that are often forgotten in the next instant paper. The analytical formalism on which I have been working on and off since my paper with the late B. E. Patchett in 1975, and to which very significant contributions have also been made by D. D. Clayton, M. G. Edmunds, F. G. A. Hartwick, R. B. Larson, D. Lynden-Bell, W. L. W. Sargent, L. Searle, B. M. Tinsley and others, is designed not only to keep the computations simple but also to introduce some order into the subject and provide the reader with an insight into what actually are the important factors in chemical evolution models, whether analytical or numerical, and which are the major uncertainties.

The book should be considered basically as a textbook suitable for beginning graduate students with a background in either physics or astronomy, but it is hoped that parts of it will also be useful to professional scientists. For this purpose, I have tried to keep the text as expository as possible with a minimum of references, but added notes at the ends of some chapters to provide a guide to the literature.

I should like to take this opportunity to thank Donald Lynden-Bell for arousing my interest in this subject and for his continued encouragement and stimulation over the years; and likewise Michael Edmunds, whose collaboration in both observational and theoretical projects has been a source of pleasure as well as (one hopes) insight. Thanks are due to them, and also to Sven Åberg, Chris Pethick and the late Roger Tayler, for helpful comments on successive versions. Finally, I warmly thank Elisabeth Grothe for her willing and expert work on the diagrams.

Bernard Pagel

Preface to the second edition

Much has happened since the book first came out in 1997. Cosmology has been transformed by balloon and satellite studies of the microwave background and by studies of distant supernovae. Host galaxies of γ-ray burst sources have been identified and some of their properties revealed. Cosmological simulations have been very successful in accounting for the large-scale structure of the Universe, although they are still challenged by observed element:element ratios suggesting that the largest galaxies were formed rapidly a long time ago, limiting the time available for their formation by mergers. The coming of 10-metre class telescopes, supplementing the Hubble Space Telescope, has led to enormous advances in abundance determinations in stars of all kinds and in galaxies, notably at high redshifts. Some stellar atmospheres can now be modelled by *ab initio* hydrodynamical simulations which account for granulation and eliminate the need for ad hoc parameters describing 'macro-turbulence' and 'micro-turbulence', leading to increasingly sophisticated abundance determinations. Nevertheless, simple analytical treatments retain their usefulness because of the insight they provide into the essential ingredients of more elaborate numerical models, whether of stellar atmospheres or of galactic chemical evolution.

I thank Monica Grady, Chris Tout and Max Pettini for critically reading through the revised Chapters 3, 5 and 12 respectively, and Mike Edmunds for continued cooperation and enlightening discussions. I owe particular thanks to my wife Annabel Tuby Pagel for her loving care during difficult times.

Bernard Pagel

1

Introduction and overview

I believe that a leaf of grass is no less than the journey work of the stars.
Walt Whitman, *Song of Myself*

1.1 General introduction

The existence and distribution of the chemical elements and their isotopes is a consequence of nuclear processes that have taken place in the past in the Big Bang and subsequently in stars and in the interstellar medium (ISM) where they are still ongoing. These processes are studied theoretically, experimentally and observationally. Theories of cosmology, stellar evolution and interstellar processes are involved, as are laboratory investigations of nuclear and particle physics, cosmochemical studies of elemental and isotopic abundances in the Earth and meteorites and astronomical observations of the physical nature and chemical composition of stars, galaxies and the interstellar medium.

Figure 1.1 shows a general scheme or 'creation myth' which summarizes our general ideas of how the different nuclear species (loosely referred to hereinafter as 'elements') came to be created and distributed in the observable Universe. Initially – in the first few minutes after the Big Bang – universal cosmological nucleosynthesis at a temperature of the order of 10^9 K created all the hydrogen and deuterium, some ^{3}He, the major part of ^{4}He and some ^{7}Li, leading to primordial mass fractions $X \simeq 0.75$ for hydrogen, $Y \simeq 0.25$ for helium and $Z = 0.00$ for all heavier elements (often loosely referred to by astronomers as 'metals'!). The existence of the latter in our present-day world is the result of nuclear reactions in stars followed by more or less violent expulsion of the products when the stars die, as first set out in plausible detail by E. M. and G. R. Burbidge, W. A. Fowler and F. Hoyle (usually abbreviated to B^{2}FH) in a classic article in *Reviews of Modern Physics* in 1957 and independently by A. G. W. Cameron in an Atomic Energy of Canada report in the same year (B^{2}FH 1957; Cameron 1957).

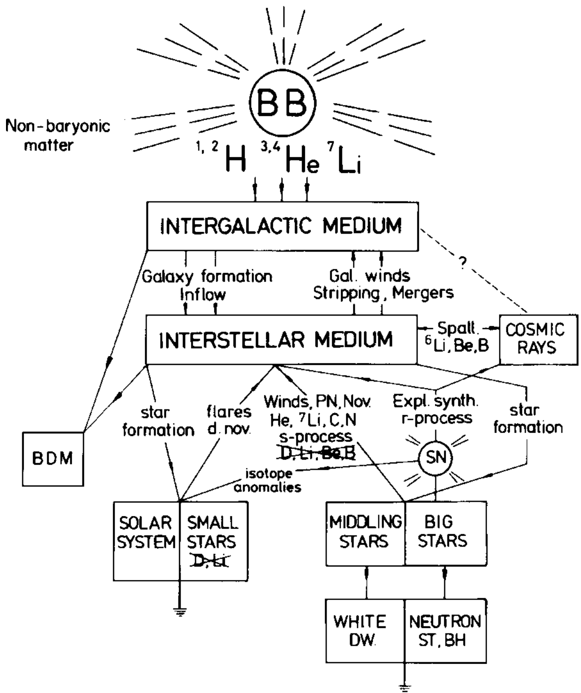

Fig. 1.1. A scenario for cosmic chemical evolution, adapted from Pagel (1981).

Estimates of primordial abundances from the Big Bang, based on astrophysical and cosmochemical observations and arguments, lead to a number of interesting deductions which will be described in Chapter 4. In particular, there are reasons to believe that, besides the luminous matter that we observe in the form of stars, gas and dust, there is dark matter detectable from its gravitational effects (including gravitational lensing). This dark matter, in turn, has two quite distinct components: one is ordinary baryonic matter, consisting of protons, neutrons and electrons, which happens not to shine detectably at accessible wavelengths. There is evidence for such baryonic dark matter (BDM) in the form of rarefied ionized intergalactic gas producing absorption lines – notably at high redshifts – and also possibly in the form of 'MACHOs' (massive compact halo objects) – stellar-mass dark objects arguably in the halo of our Galaxy detected from their gravitational micro-lensing of background sources in the Magellanic Clouds (but at least some of them are possibly normal stars in the Magellanic Clouds themselves). There could also be contributions from cold molecular hydrogen and from low surface brightness galaxies not picked up in redshift surveys.

The other kind of dark matter must be non-baryonic (NDM) and is thought to consist of some kind of particles envisaged in extensions of the 'Standard Model' of particle physics. The most popular candidates are so-called cold dark matter (CDM) particles that decoupled from radiation very early on in the history of the Universe and now have an exceedingly low kinetic temperature which favours the formation of structures on the sort of scales that are observed in galaxy redshift surveys. The seeds of those structures would have been quantum fluctuations imprinted very early (maybe $\sim 10^{-35}$ s) after the Big Bang during a so-called inflationary era of super-rapid expansion preceding the kind of expanding Universe that we experience now, which later enabled pockets of mainly dark matter slightly denser than the average to separate out from the general expansion by their own gravity. A small contribution to NDM also comes from neutrinos, since evidence for their flavour oscillations implies that they have a small mass, but this mass is estimated from microwave background data to be ≤ 0.2 eV (averaged over the three flavours) and their contribution to NDM ≤ 5 per cent.

The first few minutes are followed by a plasma phase lasting of the order of 10^5 years during which the Universe was radiation-dominated and the baryonic gas, consisting almost entirely of hydrogen and helium, was ionized and consequently opaque to radiation through electron scattering. But expansion was accompanied by cooling, and when the temperature was down to about 10^4 K (at a redshift of about 3450), matter began to dominate and at redshifts around 1100, some 370 000 years after the Big Bang (ABB), first helium and then hydrogen became neutral by recombination.[1] The Universe became transparent and background radiation was scattered for the last time (and is now received as black-body radiation with a temperature of 2.7 K) leading to a period commonly known as the 'dark ages'.[2] Eventually gas began to settle in the interiors of the pre-existing dark-matter halos, resulting in the formation of stars, galaxies and groups and clusters of galaxies, and in re-ionization of the intergalactic medium by newly formed massive stars and/or the compact ultra-luminous objects known as quasars or quasi-stellar objects (QSOs) associated with galactic nuclei.

The epoch and mode of galaxy formation are not well known, but both quasars and star-forming galaxies are known with redshifts up to about 7, corresponding to an era when the expanding Universe was only 1/8 of its present size, and the emission-line spectra of quasars indicate a large heavy-element abundance (solar or more; Hamann & Ferland 1999), suggesting prior stellar activity. The first stars, on the other hand, known as 'Population III', would have been devoid of 'metals'; whether they differed from normal stars in other basic characteristics, notably their mass distribution, is not known, since no completely metal-free stars have been

[1] Since this was the first time electrons were captured by protons and α-particles it might be more appropriate to talk about 'combination' rather than 'recombination'!

[2] 'Infrared ages' might be a more appropriate term.

found. Data from the WMAP[3] polarization measurements published in 2003 suggest that re-ionization took place over an extended period between redshifts of 30 and 10, corresponding to ages of the Universe between about 100 and 400 Myr.[4] In the most popular models, galaxies form by cooling and collapse of baryonic gas contained in non-gaseous (and consequently non-dissipative) dark-matter halos that build up from hierarchical clustering, with complications caused by mergers that may take place both in early stages and much later; these mergers (or tidal interactions) may play a significant role in triggering star formation at the corresponding times.

Galaxies thus have a mixture of stars and diffuse interstellar medium. (The diffuse ISM generally consists of gas and dust, but will often be loosely referred to hereinafter as 'gas'.) Most observed galaxies belong to a sequence first established in the 1920s and 30s by Edwin Hubble. So-called early-type galaxies according to this classification are the ellipticals, which are ellipsoidal systems consisting of old stars and relatively little gas or dust detectable at optical, infrared or radio wavelengths; they do, however, contain substantial amounts of very hot X-ray emitting gas. Later-type galaxies have a rotating disk-like component surrounding an elliptical-like central bulge, with the relative brightness of the disk increasing along the sequence. The disks display a spiral structure, typical of spiral galaxies such as our own Milky Way system, and the proportion of cool gas relative to stars increases along the sequence, together with the relative rate of formation of new stars from the gas, so that their colours become increasingly blue. At the end of the Hubble sequence are irregular galaxies, such as the Magellanic Clouds (the nearest major galaxies outside our own), and outside the sequence there is a variety of small systems known as dwarf spheroidals, dwarf irregulars and blue compact and H II (i.e. ionized hydrogen) galaxies. The last three classes actually overlap (being partly classified by the method of discovery) and they are dominated by the light of young stars and (in the case of H II and some blue compact galaxies) the gas ionized by those young stars (see Chapter 3). There are also radio galaxies and so-called Seyfert galaxies with bright nuclei that have spectra resembling those of quasars; these are collectively known as active galactic nuclei (AGNs), and are associated with large ellipticals and early-type spirals. The increase in the proportion of cool gas along the Hubble sequence could be due to differences in age, the most gas-poor galaxies being the oldest, or to differences in the rates at which gas has been converted into stars in the past or added or removed by interaction with other galaxies and the intergalactic medium (IGM), or perhaps some combination of all of these.

[3] Wilkinson Microwave Anisotropy Probe, launched in 2001.
[4] Assuming the currently favoured flat Λ-CDM cosmology with $\Omega_m = 0.24, \quad H_0 = 73\,\mathrm{km\,s^{-1}\,Mpc^{-1}}$.

The figure illustrates very schematically some possible interactions between galaxies and the intergalactic medium. The IGM can be roughly considered as a combination of a diffuse medium and discrete clouds, the latter being manifested in the local Universe by absorption lines of H I Lyman-α λ 1216 and O VI $\lambda\lambda$ 1032, 1038 detected in the far ultraviolet,[5] by high-velocity H I clouds detected from the hyperfine 21-cm transition of neutral atomic hydrogen at high Galactic latitudes (which may be of extragalactic origin in some cases, although this is quite controversial) and by hot X-ray emitting gas in clusters and groups of galaxies. H I gas is detected in disk and blue compact galaxies but no isolated intergalactic H I clouds have been found. At high redshifts, Gunn and Peterson (1965) predicted[6] that, as one looks through to the re-ionization epoch, one should see a broad absorption trough shortward of the Lyman-α emission line from a quasar, due to diffuse neutral hydrogen at a range of redshifts in the foreground. This effect was first found for the corresponding line of He^+, λ 304 (redshifted to wavelengths near 1200 Å accessible to HST[7] and FUSE), accompanied by discrete absorption lines from the knots and filaments in which most of the CDM (and associated gas) has gathered by the corresponding epoch in accordance with numerical simulations of gravitational clustering. In the case of H I, which is much less abundant owing to the ionizing radiation field at those epochs, one only sees discrete lines, called the 'Lyman-α forest', resulting from the knots and filaments, at redshifts up to 4 or so (see Figs. 4.5, 12.5), but the classical Gunn–Peterson effect of diffuse intergalactic hydrogen does appear at redshifts greater than about 6, deeper into the re-ionization epoch.

The interactions between the ISM and IGM include expulsion of diffuse material from galaxies in the form of galactic winds driven by supernova energy ('feedback'), stripping of (especially the outer) layers of the gas content of galaxies by tidal forces or by ram pressure in an intra-cluster medium when the galaxy is a member of a cluster; and/or inflow of intergalactic gas into galaxies, which latter may be manifested by some of the high-velocity H I clouds in our own Milky Way system.

Figure 1.1 also gives a schematic illustration of the complex interactions between the ISM and stars. Stars inject energy, recycled gas and nuclear reaction products ('ashes of nuclear burning') enriching the ISM from which other generations of stars form later. This leads to an increase in the heavy-element content of both the ISM and newly formed stars; the subject of 'galactic chemical evolution' (GCE) is really all about these processes. On the other hand, nuclear products may

[5] Notably by the FUSE (Far UV Spectroscopic Explorer) mission launched in 1999.
[6] Similar considerations were put forward independently by Shklovsky (1964) and Scheuer (1965).
[7] Hubble Space Telescope.

be lost from the ISM by galactic winds or diluted by inflow of relatively unprocessed material. The heavy-element content of the intra-cluster X-ray gas in rich clusters like Coma,[8] amounting to about 1/3 of solar, may have resulted from winds from the constituent galaxies (see Chapter 11), or possibly from the destruction of dwarf galaxies in the cluster.

The effects of different sorts of stars on the ISM depend on their (initial) mass and on whether they are effectively single stars or interacting binaries; some of the latter are believed to be the progenitors of Type Ia supernovae (SN Ia) which are important contributors to iron-group elements in the Galaxy. Big stars, with initial mass above about 10 $M_\odot$ ($M_\odot$ is the mass of the Sun), have short lives ($\sim$ 10 Myr), they emit partially burned material in the form of stellar winds and those that are not too massive eventually explode as Type II (or related Types Ib and Ic) supernovae, ejecting elements up to the iron group with a sprinkling of heavier elements. (Supernovae are classed as Type I or II according to whether they respectively lack, or have, lines of hydrogen in their spectra, but all except Type Ia seem to be associated with massive stars of short lifetime which undergo core collapse leading to a compact remnant.) The most massive stars of all are expected to collapse into black holes, with or without a prior supernova explosion; the upper limit for core collapse supernovae is uncertain, but it could be somewhere in the region of 50 $M_\odot$.

Middle-sized stars, between about 1 and 8 $M_\odot$, undergo complicated mixing processes and mass loss in advanced stages of evolution, culminating in the ejection of a planetary nebula while the core becomes a white dwarf. Such stars are important sources of fresh carbon, nitrogen and heavy elements formed by the slow neutron capture (s-) process (see Chapter 6). Finally, small stars below 1 $M_\odot$ have lifetimes comparable to the age of the Universe and contribute little to chemical enrichment or gas recycling and merely serve to lock up material.

The result of all these processes is that the Sun was born 4.6 Gyr ago with mass fractions $X \simeq 0.70, \; Y \simeq 0.28, \; Z \simeq 0.02$. These abundances (with perhaps a slightly lower value of Z) are also characteristic of the local ISM and young stars. The material in the solar neighbourhood is about 15 per cent ‘gas’ (including dust which is about 1 per cent by mass of the gas) and about 85 per cent stars or compact remnants thereof; these are white dwarfs (mainly), neutron stars and black holes.

1.2 Some basic facts of nuclear physics

(i) An atomic nucleus consists of Z protons and N neutrons, where Z is the *atomic number* defining the charge of the nucleus, the number of electrons in the neutral atom and hence the chemical element, and $Z + N = A$, the *mass number* of the nuclear species.

[8] The nearest rich cluster of galaxies, in the constellation Coma Berenices.

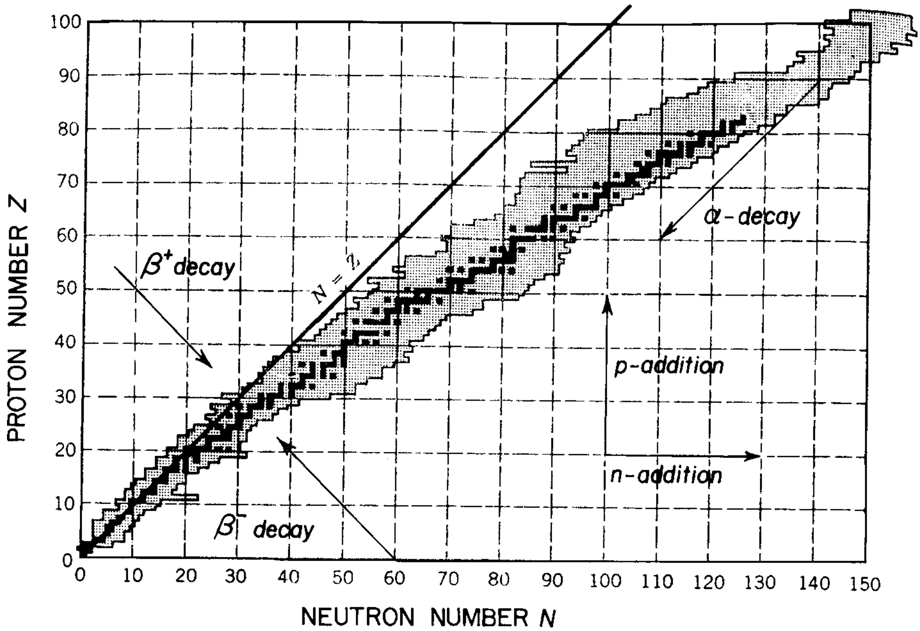

Fig. 1.2. Chart of the nuclides, in which Z is plotted against N. Stable nuclei are shown in dark shading and known radioactive nuclei in light shading. Arrows indicate directions of some simple nuclear transformations. After Krane (1987). Reproduced by permission of John Wiley & Sons, Inc.

Protons and neutrons are referred to collectively as *nucleons*. Different values of A and N for a given element lead to different *isotopes*, while nuclei with the same A and different Z are referred to as *isobars*. A given nuclear species is usually symbolized by the chemical symbol with Z as an (optional) lower and A as an upper prefix, e.g. $^{56}_{26}$Fe.

Stable nuclei occupy a 'β-stability valley' in the Z, N plane (see Fig. 1.2), where one can imagine energy (or mass) being plotted along a third axis perpendicular to the paper. Various processes, some of which are shown in the figure, transform one nucleus into another. Thus, under normal conditions, a nucleus outside the valley undergoes spontaneous decays, while in accelerators, stars and the early Universe nuclei are transformed into one another by various reactions.

(ii) The binding energy per nucleon varies with A along the stability valley as shown in Fig. 1.3, and this has the following consequences:

(a) Since the maximum binding energy per nucleon is possessed by ^{62}Ni, followed closely by ^{56}Fe, energy is released by either fission of heavier or fusion of lighter nuclei. The latter process is the main source of stellar energy, with the biggest contribution (7 MeV per nucleon) coming from the conversion of hydrogen into helium (H-burning).

(b) Some nuclei are more stable than others, e.g. the α-particle nuclei ^{4}He, ^{12}C, ^{16}O, ^{20}Ne, ^{24}Mg, ^{28}Si, ^{32}S, ^{36}Ar, ^{40}Ca. Nuclei with a couple of A-values (5 and 8) are

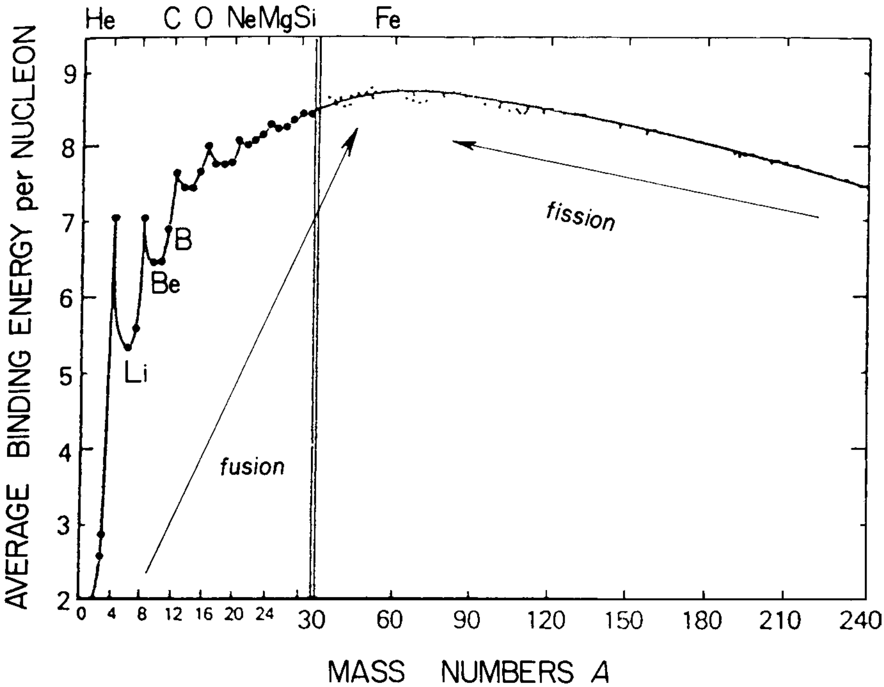

Fig. 1.3. Binding energy per nucleon as a function of mass number. Adapted from Rolfs and Rodney (1988).

violently unstable, owing to the nearby helium peak. Others are stable but only just: examples are D, ^{6,7}Li, ^{9}Be and ^{10,11}B, which are destroyed by thermonuclear reactions at relatively low temperatures.

(iii) Nuclear reactions involving charged particles (p, α etc.) require them to have enough kinetic energy to get through in spite of the electrostatic repulsion of the target nucleus (the 'Coulomb barrier'); the greater the charges, the greater the energy required. In the laboratory, the energy is supplied by accelerators, and analogous processes are believed to occur in reactions induced in the ISM by cosmic rays (see Chapter 9). In the interiors of stars, the kinetic energy exists by virtue of high temperatures (leading to *thermonuclear* reactions) and when one fuel (e.g. hydrogen) runs out, the star contracts and becomes hotter, eventually allowing a more highly charged fuel such as helium to 'burn'.

There is no Coulomb barrier for neutrons, but free neutrons are unstable so that they have to be generated *in situ*, which again demands high temperatures.

1.3 The local abundance distribution

Figure 1.4 shows the 'local Galactic' abundances of isobars, based on a combination of elemental and isotopic determinations in the Solar System with data from

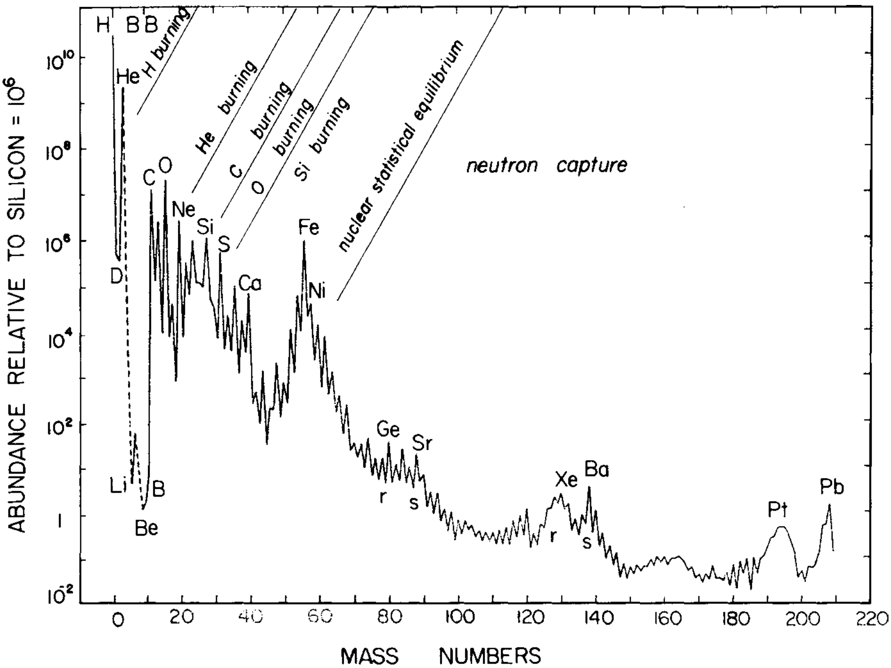

Fig. 1.4. The 'local Galactic' abundance distribution of nuclear species, normalized to 10^6 ^{28}Si atoms, adapted from Cameron (1982).

nearby stars and emission nebulae. These are sometimes referred to as 'cosmic abundances', but because there are significant variations among stars and between and across galaxies this term is best avoided. The curve shows a number of features that give clues to the origin of the various elements:

(i) Hydrogen is by far the most abundant element, followed fairly closely by helium. This is mainly formed in the Big Bang, with some topping up of the primordial helium abundance ($Y_P \simeq 0.25$) by subsequent H-burning in stars ($Y \simeq 0.28$ here and now). Only a small fraction ($Z \simeq 0.02$) of material in the ISM and in newly formed stars has been subjected to high enough temperatures and densities to burn helium.

(ii) The fragile nuclei Li, Be and B are very scarce, being destroyed in the harsh environment of stellar interiors, although some of them may also be created there. (The lithium abundance comes from measurements in meteorites; it is still lower in the solar photosphere because of destruction by mixing with hotter layers below.) On the other hand, they are much more abundant in primary cosmic rays as a result of $\alpha - \alpha$ fusion and spallation reactions between p, α and (mainly) CNO nuclei at high energies. The latter may also account for the production of some of these species in the ISM. Some ^{7}Li (about 10 per cent) is also produced in the Big Bang.

(iii) Although still more fragile than Li, Be and B, deuterium is vastly more abundant (comparable to Si and S). D is virtually completely destroyed in gas recycled through stars and there are no plausible mechanisms for creating it there in such quantities, but it is nicely accounted for by the Big Bang. The observed abundance is a lower limit to the primordial abundance. The light helium isotope ^{3}He is the main product when deuterium is destroyed and can also be freshly produced in stars as well as destroyed. It has comparable abundance to D and some is made in the Big Bang, but in this case the interpretation of the observed abundance is more complicated.

(iv) Nuclei from carbon to calcium show a fairly regular downward progression modulated by odd:even and shell effects in nuclei which affect their binding energy (see Chapter 2). These are produced in successive stages of stellar evolution when the exhaustion of one fuel is followed by gravitational contraction and heating enabling the previous ashes to 'burn'. The onset of carbon burning, which leads to Mg and nearby elements, is accompanied by a drastic acceleration of stellar evolution due to neutrino emission caused by lepton and plasma processes at the high densities and temperatures required for such burning. The neutrinos directly escape from the interior of the star, in contrast to photons for which it takes of the order of 10^5 yr for their energy to reach the surface, and they eventually carry away energy almost as fast as it is generated by nuclear reactions; it is this rapid loss of energy[9] that speeds up the stellar evolution (see Chapter 5).[10]

(v) The iron-group elements show an approximation to nuclear statistical equilibrium at a temperature of several $\times\, 10^9$ K or several tenths of an MeV leading to the iron peak. This was referred to by B^{2}FH as the 'e-process' referring to thermodynamic equilibrium. Because the reactions are fast compared to β-decay lifetimes, the overall proton:neutron ratio remains fixed so that complete thermodynamic equilibrium does not apply here, but one has an approach to statistical equilibrium in which forward and reverse nuclear reactions balance. The iron peak in the abundance distribution is thought to result from explosive nucleosynthesis which may occur in one or other of two typical situations. One of these involves the shock that emerges from the core of a massive star that has collapsed into a neutron star; heat from the shock ignites the overlying silicon and oxygen layers in a Type II (or related) supernova outburst, and they are expelled with the aid of energetic neutrinos from the collapsed object ('neutrino heating' or 'drag'). Another possible cause is the sudden ignition of carbon in a white dwarf that has accreted enough material from a companion to bring it close to or over the Chandrasekhar mass limit (supernova Type Ia, often referred to as 'thermonuclear'). In either case, the quasi-equilibrium is frozen at a distribution characteristic of the highest temperature reached in the shock before the material is cooled by expansion, but the initial proton:neutron ratio is another important parameter. Calculations and observations both indicate that the dominant product is actually

[9] Sometimes referred to as 'neutrino cooling', although it does not in general lead to lower temperatures.

[10] Neutrinos are also generated by purely nuclear processes involving weak interactions, e.g. in the Sun. Such neutrinos can be an important cause of energy losses in compact stars through the 'Urca' process, in which an inverse β-decay is followed by a normal β-decay resulting in a neutrino–antineutrino pair.

^{56}Ni, the 'doubly magic' nucleus with equal numbers of protons and neutrons, which later decays via ^{56}Co into ^{56}Fe.

(vi) Once iron-group elements have been produced, all nuclear binding energy has been extracted and further gravitational contraction merely leads to photo-disintegration of nuclei with a catastrophic consumption of energy. This is one of several mechanisms that either drive or accelerate core collapse. By contrast, the thermonuclear explosion of a white dwarf simply leads to disintegration of the entire star.

Consequently, charged-particle reactions do not lead to significant nucleosynthesis beyond the iron group and the majority of heavier nuclei result from neutron captures. One or more such captures on a seed nucleus (in practice mostly ^{56}Fe) lead to the production of a β-unstable nucleus (e.g. ^{59}Fe) and the eventual outcome then depends on the relative timescales for neutron addition and β-decay. In the slow or s-process, neutrons are added so slowly that most unstable nuclei have time to undergo β-decay and nuclei are built up along the stability valley in Fig. 1.2 up to ^{209}Bi, whereafter α-decay terminates the process. In the rapid or r-process, the opposite is the case and many neutrons are added under conditions of very high temperature and neutron density, building unstable nuclei up to the point where (n, γ) captures are balanced by (γ, n) photo-disintegrations leading to a kind of statistical equilibrium modified by (relatively slow) β-decays. Eventually (e.g. after a SN explosion), the neutron supply is switched off and the products then undergo a further series of β-decays ending up at the nearest stable isobar, which will be on the neutron-rich side of the β-stability valley (Fig. 1.5). Some species have contributions from both r- and s-processes, while others are pure r (if by-passed by the s-process) or pure s (if shielded by a more neutron-rich stable isobar); the actinides (U, Th etc.) are pure r-process

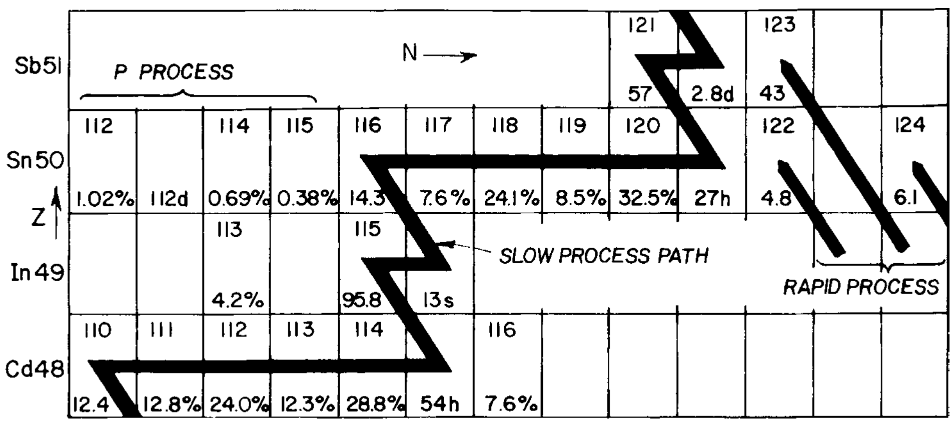

Fig. 1.5. Paths of the r-, s- and p-processes in the neighbourhood of the tin isotopes. Numbers in the boxes give mass numbers and percentage abundance of the isotope for stable species, and β-decay lifetimes for unstable ones. ^{116}Sn is an s-only isotope, shielded from the r-process by ^{116}Cd. After Clayton *et al.* (1961). Copyright by Academic Press, Inc. Courtesy Don Clayton.

products. A few species on the proton-rich side of the stability valley are not produced by neutron captures at all and are attributed to what B^2FH called the 'p-process'; these all have very low abundances and are believed to arise predominantly from (γ, n) photo-disintegrations of neighbouring nuclei.

Neutron capture processes give rise to the so-called magic-number peaks in the abundance curve, corresponding to closed shells with 50, 82 or 126 neutrons (see Chapter 2). In the case of the s-process, the closed shells lead to low neutron-capture cross-sections and hence to abundance peaks in the neighbourhood of Sr, Ba and Pb (see Fig. 1.4), since such nuclei will predominate after exposure to a chain of neutron captures. In the r-process, radioactive progenitors with closed shells are more stable and hence more abundant than their neighbours and their subsequent decay leads to the peaks around Ge, Xe and Pt on the low-A side of the corresponding s-process peak.

1.4 Brief outline of stellar evolution

(i) An interstellar cloud collapses forming a generation of stars. The masses of the stars are spread over a range from maybe $0.01\,M_\odot$ or less to maybe $100\,M_\odot$ or so. The distribution function of stellar masses at birth, known as the 'initial mass function' (IMF), has more small stars than big ones.

(ii) The young stars, which appear as variable stars with emission lines known as T Tauri stars and related classes, initially derive their energy from gravitational contraction, which leads to a steady increase in their internal temperature (see Chapter 5). Eventually the central temperature becomes high enough ($\sim 10^7$ K or 1 keV) to switch on hydrogen burning and the star lies on the 'zero-age main sequence' (ZAMS) of the Hertzsprung–Russell (HR) diagram in which luminosity is plotted against surface temperature (Fig. 1.6). Stars spend most of their lives (about 80 per cent) in a main-sequence band stretching slightly upwards from the ZAMS; the corresponding time is short (a few $\times\ 10^6$ years) for the most massive and luminous stars and very long ($>10^{10}$ years) for stars smaller than the Sun, because the luminosity varies as a high power of the mass and so bigger stars use up their nuclear fuel supplies faster.

(iii) When hydrogen in a central core occupying about 10 per cent of the total mass is exhausted, there is an energy crisis. The core, now consisting of helium, contracts gravitationally, heating a surrounding hydrogen shell, which consequently ignites to form helium and gradually eats its way outwards (speaking in terms of the mass coordinate). At the same time, the envelope expands, making the star a red giant in the upper right part of the diagram.

(iv) Eventually, the contracting core becomes hot enough to ignite helium ($3\alpha \rightarrow {}^{12}C$; ${}^{12}C + {}^4He \rightarrow {}^{16}O$) and the core contraction is halted.

(v) In sufficiently big stars ($>\sim 10\,M_\odot$) this process repeats; successive stages of gravitational contraction and heating permit the ashes of the previous burning stage to be

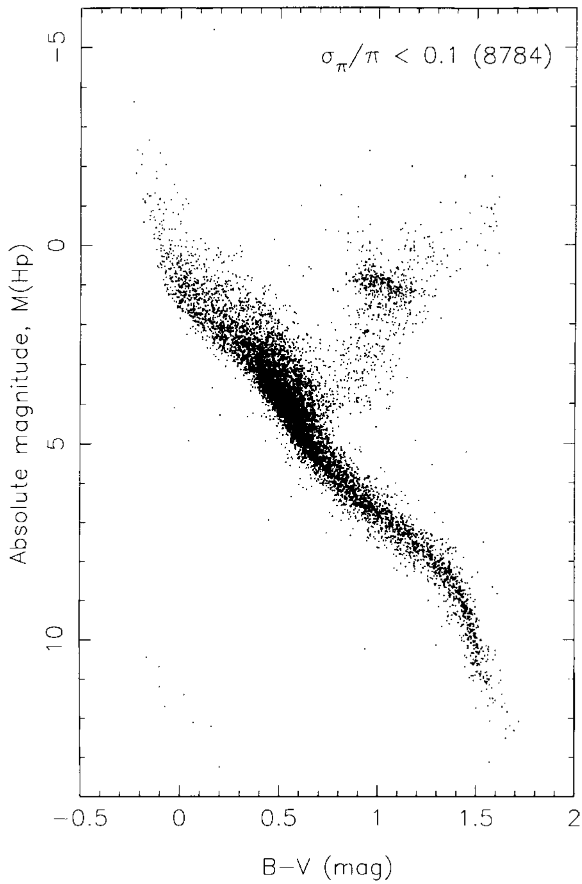

Fig. 1.6. HR diagram for nearby stars with well-known parallaxes (i.e. distances) from the HIPPARCOS astrometric satellite mission, after Perryman *et al.* (1995). The abscissa, B (blue)−V (visual) magnitude is a measure of 'redness' or inverse surface temperature ranging from about 2×10^4 K on the left to about 3000 K on the right, while the ordinate measures luminosity in the visual band expressed by absolute magnitude M_{Hp} in the HIPPARCOS photometric system. Luminosity decreases by a factor of 100 for every 5 units increase in M and the Sun's $M_V \simeq M_{\mathrm{Hp}}$ is 4.8. The main sequence forms a band going from top left to bottom right in the diagram, with the ZAMS forming a lower boundary. Subgiants and red giants go upward and to the right from the MS and a few white dwarfs can be seen at the lower left. Courtesy Michael Perryman.

ignited leading to C, Ne, O and Si burning in the centre with less advanced burning stages in surrounding shells leading to an onion-like structure with hydrogen-rich material on the outside. Silicon burning leads to a core rich in iron-group elements and with a temperature of the order of 10^9 K, i.e. about 100 keV.

(vi) The next stage of contraction is catastrophic, partly because all nuclear energy supplies have been used up when the iron group is reached, and partly because the core, having reached nearly the Chandrasekhar limiting mass for a white dwarf supported by electron degeneracy pressure, is close to instability and also suffers loss of pressure due to neutronization by inverse β-decays. Further contraction leads to photo-disintegration, which absorbs energy, and this leads to dynamical collapse of the core which continues until it reaches nuclear density and forms a neutron star. (If the mass of collapsing material is too large, then a black hole will probably form instead.) The stiff equation of state of nuclear matter leads to a bounce which sends a shock out into the surrounding layers. This heats them momentarily to high temperatures, maybe 5×10^9 K in the silicon layer, leading to explosive nucleosynthesis of iron-peak elements, mainly ^{56}Ni

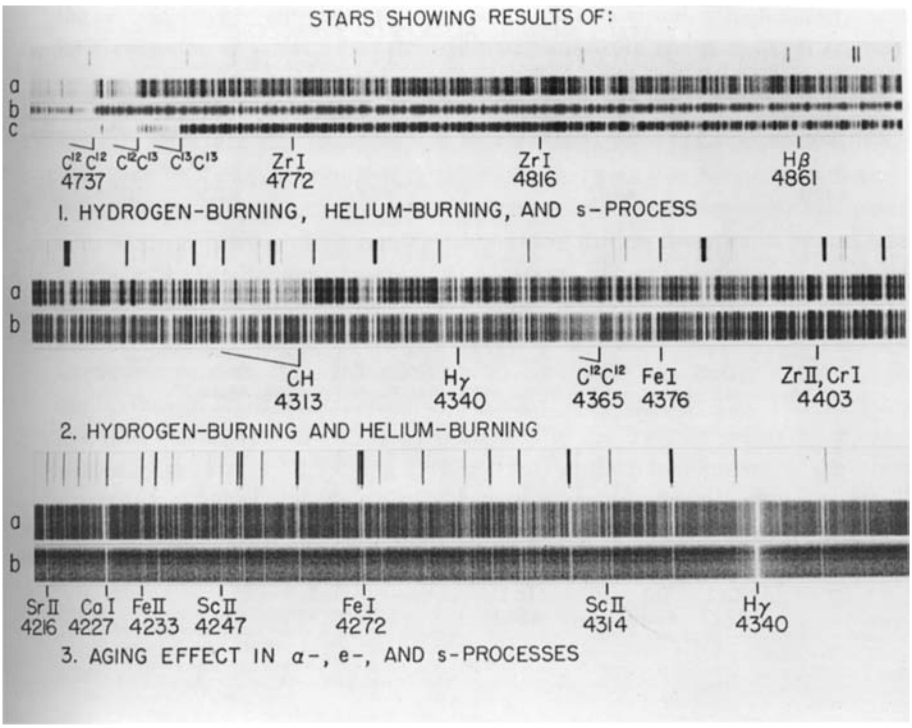

Fig. 1.7. Photographic (negative) spectra of stars showing various aspects of nucleosynthesis. Top: (a) carbon star X Cancri with ^{12}C/^{13}C $\simeq$ 4 from H-burning by the CNO cycle and a suggestion of enhanced Zr; (b) peculiar carbon star HD 137613 without ^{13}C bands in which hydrogen is apparently weak (H-deficient carbon star); (c) carbon star HD 52432, with ^{12}C/^{13}C $\sim$ 4. Middle: (a) normal carbon star HD 156074, showing the CH band and Hγ; (b) peculiar (H-poor) carbon star HD 182040 showing C_2 but weak Hγ and CH. Bottom: (a) normal F-type star ξ Pegasi (slightly hotter than the Sun); (b) old Galactic halo population star HD 19445 with similar temperature (shown by Hγ) but very low metal abundance (about 1/100 solar). After Burbidge, Burbidge, Fowler and Hoyle (B^{2}FH 1957). Courtesy Margaret and Geoffrey Burbidge.

(which later decays by electron capture and β^+ to ^{56}Fe); more external layers are heated to lower temperatures resulting in milder changes. Assisted by high-energy neutrinos, the shock expels the outer layers in a supernova explosion (Type II and related classes); the ejecta eventually feed the products into the ISM which thus becomes enriched in 'metals' in course of time. This scenario was first put forward in essentials by Hoyle (1946), and modern versions give a fairly good fit to the local abundances of elements from oxygen to calcium. The iron yield is uncertain because it depends on the mass cut between expelled and infalling material in the silicon layer, but can be parameterized to fit observational data, e.g. for SN 1987A in the Large Magellanic Cloud (LMC). The upshot is that iron-group elements are probably underproduced relative to local abundances, but the deficit is plausibly made up by contributions from supernovae of Type Ia. A subset of Type II supernovae may also be the site of the r-process (see Chapter 6).

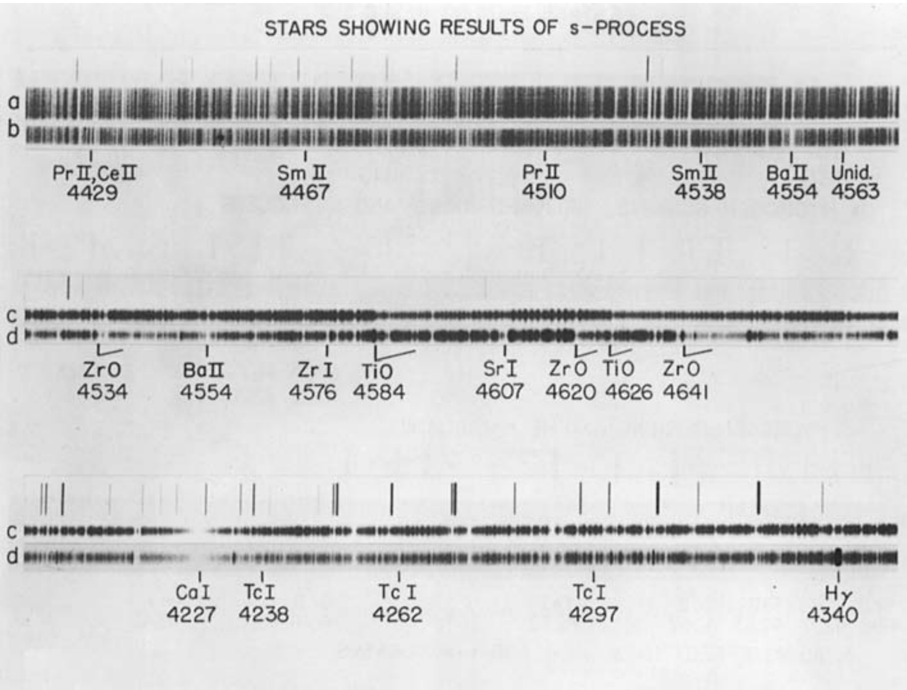

Fig. 1.8. Spectra showing effects of s-process. Top: (a) normal G-type giant κ Gem (similar temperature to the Sun); (b) Ba II star HD 46407, probably not an AGB star but affected by a companion which was. Middle: (c) M-type giant 56 Leo, showing TiO bands; (d) S-type AGB star R Andromedae showing ZrO bands, partly due to enhanced Zr abundance. Bottom: another spectral region of the same two stars showing Tc features in R And which indicate s-processing and dredge-up within a few half-lives of technetium 99 (2×10^5 yr) before the present. After B^{2}FH (1957). Courtesy Margaret and Geoffrey Burbidge.

(vii) For intermediate-mass stars (IMS), $\sim 1\,M_\odot \leq M \leq\sim 8\,M_\odot$, stages (i) to (iii) are much as before, but these never reach the stage of carbon burning because the carbon–oxygen core becomes degenerate first by virtue of high density, and later evolution is limited by extensive mass loss from the surface. After core helium exhaustion, these stars re-ascend the giant branch along the so-called asymptotic giant branch (AGB) track (see Fig. 5.15) with a double shell source: helium-burning outside the CO core and hydrogen-burning outside the He core. This is an unstable situation giving rise to thermal pulses or 'helium shell flashes' in which the two sources alternately switch on and off driving inner and outer convection zones (in which mixing takes place) during their active phases (see Chapter 5). The helium-burning shell generates ^{12}C and neutrons, either from $^{22}Ne(\alpha, n)^{25}Mg$ or from $^{13}C(\alpha, n)^{16}O$, leading to s-processing, and the products are subsequently brought up to the surface in what is known as the third dredge-up process. This process leads to observable abundance anomalies in the spectra of AGB stars: carbon and S stars; see Figs. 1.7, 1.8. The products are then ejected into the ISM by mass loss in the form of stellar winds and planetary nebulae (PN), leaving a white dwarf as the final remnant. If the white dwarf is a member of a close binary system, it can occasionally be 'rejuvenated' by accreting material from its companion, giving rise to cataclysmic variables, novae and supernovae of Type Ia (see Chapter 5).

2

Thermonuclear reactions

Wie kann man einen Helium-Kern im Potenzial-Topf kochen?
R. d'E. Atkinson and F. G. Houtermans (1928),
paraphrased in Gamow and Critchfield (1949).

2.1 General properties of nuclei

Nuclear matter has an approximately constant density, the nuclear radius being about $R_0 A^{1/3}$ where $R_0 \simeq 1.2\,\mathrm{fm}$ (1 fm, Fermi or femtometre = 10^{-13} cm) and the density $2.3 \times 10^{14}\,\mathrm{gm\,cm^{-3}}$ or $0.14\,\mathrm{amu\,fm^{-3}}$ (the atomic mass unit, amu, is defined as 1/12 of the mass of a neutral ^{12}C atom). R_0 is of the order of the Compton wavelength of the π meson, $\hbar/m_\pi c = 1.4\,\mathrm{fm}$. Some properties of nuclei can be explained on the basis of Niels Bohr's 'liquid drop' model, but others depend on the very complicated many-body effects of interactions among the constituent nucleons. These, in turn, are partially explained by the shell model, in which each nucleon is assumed to move in the mean field caused by all the others and has quantum numbers analogous to those of electrons in an atom. Gross features of the β-stability valley (Fig. 1.2) and the binding-energy curve (Fig. 1.3) are summarized in the semi-empirical mass formula originally due to C. F. von Weizsäcker

$$M(A, Z) = Zm(^1\mathrm{H}) + (A - Z)m_n - \mathrm{B.E.}/c^2, \tag{2.1}$$

where M is the mass of the neutral atom, B.E. is the total binding energy, $c^2 = 931.5\,\mathrm{MeV\,amu^{-1}}$, and

$$\begin{aligned}\mathrm{B.E.} \;\simeq\; & a_v A - a_s A^{2/3} - a_c Z(Z-1)A^{-1/3} - a_{sym}\frac{(A-2Z)^2}{A} \\ & + \frac{1+(-1)^A}{2}(-1)^Z a_p\, A^{-3/4}.\end{aligned} \tag{2.2}$$

Here $a_v \simeq 15.5\,\mathrm{MeV}$ represents a constant term in B.E. per nucleon, $a_s \simeq 16.8\,\mathrm{MeV}$ provides a surface term allowing for a reduced contribution to B.E. from nucleons at the surface and $a_c \simeq 0.72\,\text{MeV} \simeq 0.6e^2/R_0$ allows for the electrostatic repulsion of the protons. $a_{sym} \simeq 23\,\text{MeV}$ gives a term favouring equal numbers of protons and neutrons, especially at low A, which arises in part from the Pauli Exclusion Principle and in part from symmetry effects in the interaction between nucleons. The last term, with $a_p \simeq 34\,\text{MeV}$, comes from a 'pairing force' due to the propensity of identical particles to form pairs with opposite spins. This last term permits several stable isobars to exist for even A.

To the extent that the nuclear potential is central, each nucleon has an orbital angular momentum $\boldsymbol{\ell}$ as well as a spin $\mathbf{s}$, where $s = 1/2$, and total angular momentum $\mathbf{j}$. These combine by $j - j$ coupling to form the total nuclear 'spin' $\mathbf{I}$. Nuclear states are specified by their energy (relative to the ground state), and their spin and parity I^π, e.g. 0^+, where $\pi = (-1)^{\sum \ell}$. Because the individual j's of nucleons are half-integral, I is always an integer for even A and half-integral for odd A. The nuclear force is almost charge-independent, but depends on the relative orientation of particle spins and has a small non-central or tensor component. The force is of short range, overcoming the Coulomb repulsion of protons at distances $\sim R_0$, but becomes highly repulsive at shorter distances $< 0.5\,\text{fm}$ maintaining a nearly constant nuclear density.

Many significant properties of nuclear states are explained by the shell model, for which Maria G. Mayer and Hans Jensen shared the 1963 Nobel prize. This is patterned after the shell model of the atom, in which electrons fill consecutively the lowest lying available bound states and it is assumed that each nucleon effectively moves in a spherically symmetrical mean potential $V(r)$, giving it a definite orbital angular momentum quantum number ℓ and a quantum number n related to the number of nodes in the radial wave function. For the Coulomb potential, which does not apply here, the energy depends uniquely on the principal quantum number $N = n + \ell$. In the more general case, the energy depends on both n and ℓ, and n is simply used as a label to indicate successively higher energy states (starting with $n = 1$) for given ℓ, so we can have (using atomic notation) $1s, 2s \ldots, 1p, 2p \ldots$ etc.

Some simple models for $V(r)$ are shown in Fig. 2.1. Two crude approximations, the infinite square well (ISW) and the 3-dimensional harmonic oscillator (3DHO), have the advantage of leading to analytical solutions of the Schrödinger equation which lead to the following energy levels:

For ISW ($V = -V_0$ for $r < R$; $V = \infty$ for $r > R$), Clayton (1968) has given the approximation

$$E(n, \ell) \simeq -V_0 + \frac{\hbar^2}{2mR^2}\left[\pi^2\left(n + \frac{\ell}{2}\right)^2 - \ell(\ell + 1)\right], \tag{2.3}$$

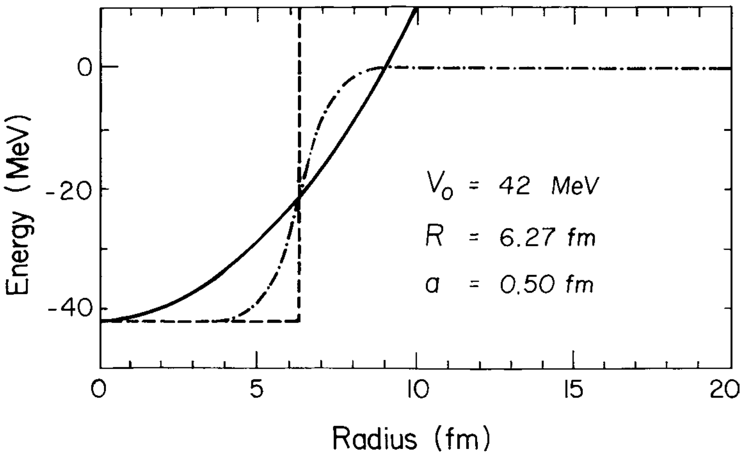

Fig. 2.1. Approximate potentials for the nuclear shell model. The solid curve represents the 3-dimensional harmonic oscillator potential, the dashed curve the infinite square well and the dot-dashed curve a more nearly realistic Woods–Saxon potential, $V(r) = -V_0/[1 + \exp\{(r - R)/a\}]$ (Woods & Saxon 1954). Adapted from Cowley (1995).

whereas for 3DHO ($V = -V_0 + \frac{1}{2}m\omega^2 r^2$),

$$E(n, \ell) = -V_0 + \hbar\omega\left(2n + \ell - \frac{1}{2}\right) \tag{2.4}$$

and the levels are highly degenerate. Figure 2.2 shows the resulting energy levels for the two cases, in which distinct energy gaps appear corresponding to closed shells of either protons or neutrons, each of which separately obey the Pauli principle. A more realistic form for $V(r)$ leads to energy levels intermediate between the two, shown on the left side of Fig. 2.3, but the higher cumulative occupation numbers above 20 do not correspond to reality. The solution to this problem came from the inclusion of a spin–orbit potential, analogous to the spin–orbit interaction that causes fine structure in atomic spectra, but in this case not of electromagnetic origin. Thus each (n, ℓ) level is split into two, with $j = \ell + s$ and $j = \ell - s$ respectively, and the splitting is proportional to $\boldsymbol{\ell}.\mathbf{s}$, for which the expectation value can be calculated by an elementary argument:

Since

$$\mathbf{j}^2 = (\boldsymbol{\ell} + \mathbf{s})^2 = \boldsymbol{\ell}^2 + 2\boldsymbol{\ell}.\mathbf{s} + \mathbf{s}^2, \tag{2.5}$$

$$\boldsymbol{\ell}.\mathbf{s} = \frac{1}{2}(\mathbf{j}^2 - \boldsymbol{\ell}^2 - \mathbf{s}^2) \tag{2.6}$$

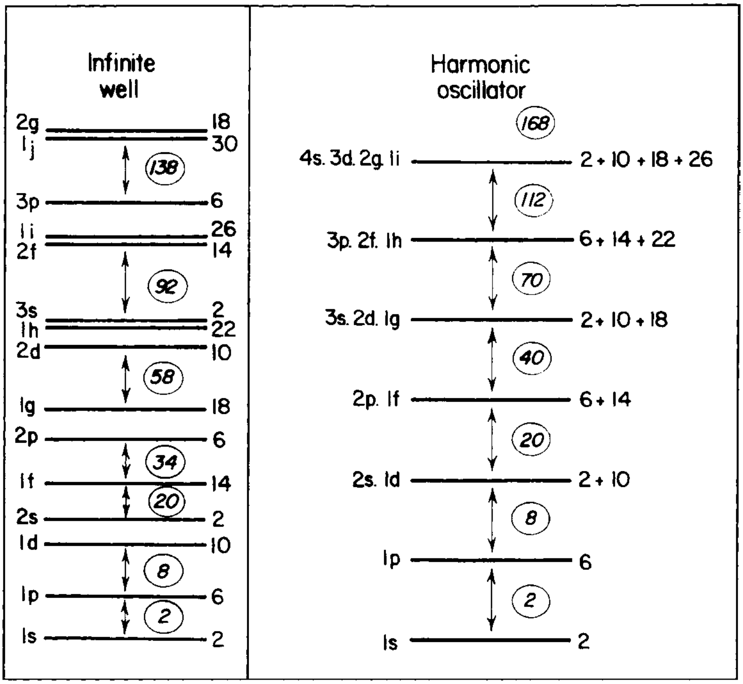

Fig. 2.2. Energy levels for ISW and 3DHO potentials. Each shows major gaps corresponding to closed shells and the numbers in circles give the cumulative number of protons or neutrons allowed by the Pauli principle. In a more realistic potential, the levels for given (n, ℓ) are intermediate between these extremes, in which the lower magic numbers 2, 8 and 20 are already apparent. Adapted from Krane (1987).

and its expectation value (in units of $\hbar^2$) is

$$\langle \boldsymbol{\ell}.\mathbf{s} \rangle = \frac{1}{2}\,[j(j+1) - \ell(\ell+1) - s(s+1)], \tag{2.7}$$

whence

$$\langle \boldsymbol{\ell}.\mathbf{s} \rangle_{\ell+1/2} - \langle \boldsymbol{\ell}.\mathbf{s} \rangle_{\ell-1/2} = \frac{1}{2}(2\ell+1) \tag{2.8}$$

so that the splitting increases with ℓ. Taking the higher j value to correspond to the lower energy (i.e. a negative coefficient of $\boldsymbol{\ell}.\mathbf{s}$ in the energy term, specifically $-13A^{-2/3}$ MeV) gives the correct magic numbers for shell closures shown on the right side of Fig. 2.3.

These shell closures have a profound influence on nuclear properties, in particular the binding energy (adding terms not accounted for in Eq. 2.2), particle separation energies and neutron capture cross-sections. The shell model also forms a basis for predicting the properties of nuclear energy levels, especially the ground

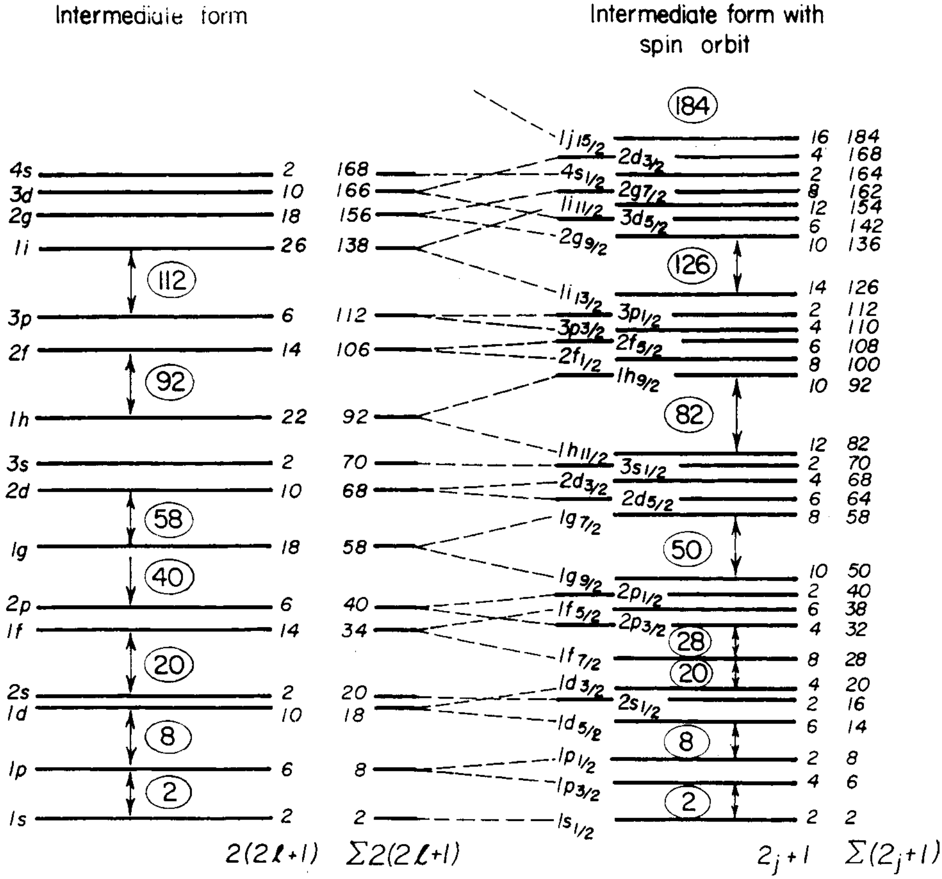

Fig. 2.3. At left, energy levels for a Woods–Saxon potential with $V_0 \simeq 50\,\text{MeV}$, $R = 1.25A^{1/3}$ fm and $a = 0.524$ fm, neglecting spin–orbit interaction. At right, the same with spin–orbit term included. Adapted from Krane (1987).

states. For even-A, even-Z nuclei, the pairing effect expressed by the a_{sym} term in Eq. (2.2) combines with the j-dependence of the energy levels to make all their ground states 0^+. For even-A, odd-Z nuclei, on the other hand, the extra proton and neutron have an overall symmetrical wave function in their respective coordinates (leading to a more compact wave function and hence lower energy than an anti-symmetrical one), with parallel spins. Thus among the few stable even-A, odd-Z nuclei (^{2}H, ^{6}Li, ^{10}B, ^{14}N), three have 1^+ ground states, while ^{10}B has 3^+.

In the case of odd-A nuclei, I^π in the ground state is fixed by the single 'valency' nucleon in the lowest vacant level shown in Fig. 2.3. In ^{15}O, for example, 8 protons fill closed shells up to $1p_{1/2}$, 6 neutrons fill closed shells up to $1p_{3/2}$ and the last neutron occupies $1p_{1/2}$ making the state $\frac{1}{2}^-$. In ^{17}O, on the other hand, all states up to $1p_{1/2}$ are filled by both protons and neutrons and the extra neutron occupies

$1d_{5/2}$, making the state $\frac{5}{2}^+$. These rules are generally valid for $A < 150$ and $190 < A < 220$; outside these ranges, cooperative effects of many single-particle shell-model states may combine to produce a permanent nuclear deformation, and even within them the single-particle shell model does not account for all excited states. A more general classification uses the concept of isospin which treats protons and neutrons as states of a single nucleon with $+1/2$ and $-1/2$ components along the z-axis of a spin-like vector in an abstract space.

2.2 Nuclear reaction physics

Typical reactions relevant to astrophysics are

- H-burning in the Big Bang ($T \simeq 10^9$ K, $kT \simeq 0.1$ MeV) and in stars (10^7 K $< T < 10^8$ K, 1 keV $< kT <$ 10 keV).
- He-burning in stars ($T \simeq 10^8$ K, $kT \simeq 10$ keV).
- C-, Ne-, O-burning in stars (10^8 K $< T < 10^9$ K, 10 keV $< kT < 0.1$ MeV).
- Si-burning, hydrostatically near 10^9 K (0.1 MeV) and explosively at several times 10^9 K.
- Neutron capture in the Big Bang, s-process (a few $\times 10^8$ K) and r-process (a few $\times$ 10^9 K).
- Spallation reactions, especially those involving cosmic rays in the ISM (non-thermal, with MeV to GeV energies). Spallation reactions are those in which one or a few nucleons are split off from a nucleus (see Chapter 9).

Figure 2.4 illustrates two kinds of generic nuclear reaction. A target labelled '1', which is in its ground state, is impacted by a projectile '2' with initial kinetic energy E in the centre-of-mass (CM) coordinate system, leading to a product '3' and ejecta '4' with energy E'. The reaction is summarized in compact notation as 1(2,4)3, e.g. $^{15}\mathrm{N}(p,\alpha)^{12}\mathrm{C}$. The energy released, $E' - E$, is usually called Q, and

$$Q = c^2(M_1 + M_2 - M_3 - M_4), \tag{2.9}$$

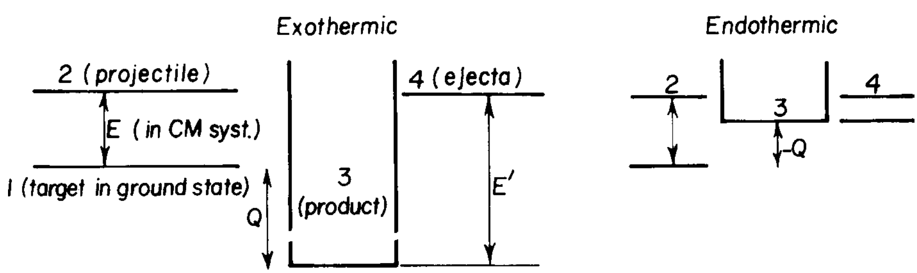

Fig. 2.4. Schematic illustration of a generic nuclear reaction.

where $c^2 = 931.5\,\mathrm{MeV\,amu^{-1}}$ and the reaction is said to be exothermic or endothermic according to whether Q is positive or negative. The value of Q can be deduced from tables of nuclear masses, and the CM kinetic energy is $\frac{1}{2}mv^2$, where m is the reduced mass $M_1M_2/(M_1 + M_2)$ and v the relative velocity, since relativistic effects are negligible for nuclear particles at the relevant energies. Nuclear reactions are subject to the standard conservation laws in addition to that of mass–energy, i.e. conservation of linear and angular momentum, parity, baryon and lepton numbers and isospin, except that parity and isospin are not always conserved in weak interactions.

The probability of a particular reaction (or scattering) taking place is measured by the relevant cross-section, which can be thought of in classical terms as the cross-sectional area of a sphere that has the same probability of being hit. The corresponding nuclear dimensions would be of order

$$\begin{aligned} \pi(R_1 + R_2)^2 &= \pi[1.2 \times 10^{-13}(A_1^{1/3} + A_2^{1/3})\,\mathrm{cm}]^2 \\ &= 4.5 \times 10^{-26}(A_1^{1/3} + A_2^{1/3})^2\ \mathrm{cm}^2 \\ &\sim 10^{-24}\ \mathrm{cm}^2 \equiv 1\,\mathrm{barn}, \end{aligned} \tag{2.10}$$

but at relevant energies the cross-section is in fact related to the de Broglie wavelength and mutual orbital angular momentum of the particles. The incoming particle is represented quantum-mechanically as a plane wave which in turn can be decomposed into a series of spherical waves characterized by their angular momentum quantum number ℓ, corresponding to an impact parameter r_ℓ where

$$mv\,r_\ell = \ell\hbar, \tag{2.11}$$

i.e. the impact parameters are quantized in units of the reduced de Broglie wavelength $\bar{\lambda} = \hbar/mv$. A semi-classical interpretation is that the plane of impact parameters is divided into zones of differing values of ℓ as shown in Fig. 2.5. The area of the ℓth zone, which is the total cross-section for given ℓ, is then

$$\pi(\hbar/mv)^2\,[(\ell+1)^2 - \ell^2] = \pi(\hbar/mv)^2\,(2\ell+1). \tag{2.12}$$

Thus for an s-wave ($\ell = 0$), which corresponds to hitting the bull's eye and so usually dominates unless forbidden by selection rules or upstaged by a resonance, the total cross-section (of which the major component is normally elastic scattering) is given by

$$\sigma_{1,2\,tot} = (1 + \delta_{12})\pi\bar{\lambda}^2 = (1 + \delta_{12})\frac{65.7}{AE}\ \mathrm{barn}, \tag{2.13}$$

where A is the reduced mass in amu and E in keV. The factor $(1+\delta_{12})$ comes from the fact that, when two identical particles interact, the cross-section is doubled because either of them can be identified as the projectile or as the target. Actual

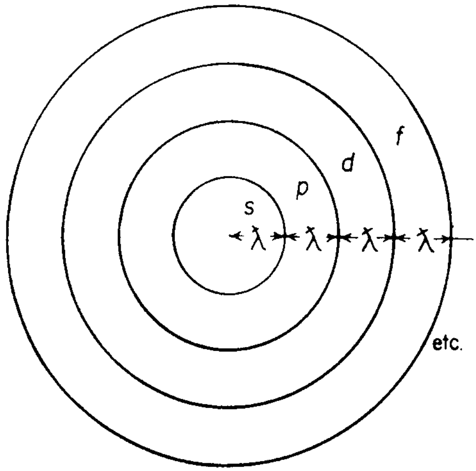

Fig. 2.5. Dependence of total reaction cross-section on the angular momentum quantum number.

cross-sections vary widely according to the nature of the interaction involved, e.g. for $E = 2\,\mathrm{MeV}$ some characteristic cross-sections are as follows:

- for $^{15}\mathrm{N}(p, \alpha)^{12}\mathrm{C}$, $\sigma = 0.5\,\mathrm{b}$ (strong nuclear force);
- for $^{3}\mathrm{He}(\alpha, \gamma)^{7}\mathrm{Be}$, $\sigma \simeq 10^{-6}\,\mathrm{b}$ (electromagnetic interaction);
- for $p(p, e^{+}\nu)d$, $\sigma \simeq 10^{-20}\,\mathrm{b}$ (weak force, based on theoretical calculations, since the rate is too small to be measured).

2.3 Non-resonant reactions

Reactions may be either 'direct', where an energetic particle has such a small wavelength that it only 'sees' one nucleon of the target, or 'compound nucleus' reactions, where the projectile's energy is shared among many nucleons in successive collisions within a compound nucleus which can then decay into one of a number of 'exit channels' (Fig. 2.6). The first case is the more common one in reactions between light nuclei, whereas the second dominates for heavier ones.

A compound-nucleus reaction can be described as

$$1 + 2 \rightarrow C \rightarrow 3 + 4 + Q \tag{2.14}$$

and the cross-section results from the joint probability that the compound nucleus is formed from $1 + 2$ and that it then decays into the channel $3 + 4$, i.e.

$$\sigma = \sigma_{tot}\, \omega \mid \langle 3, 4 \mid H_{II} \mid C \rangle \langle C \mid H_{I} \mid 1, 2 \rangle \mid^2, \tag{2.15}$$

where $\omega = (2I_3 + 1)(2I_4 + 1)/[(2I_1 + 1)(2I_2 + 1)]$ is the statistical-weight factor (obtained by averaging over initial states and summing over final states).

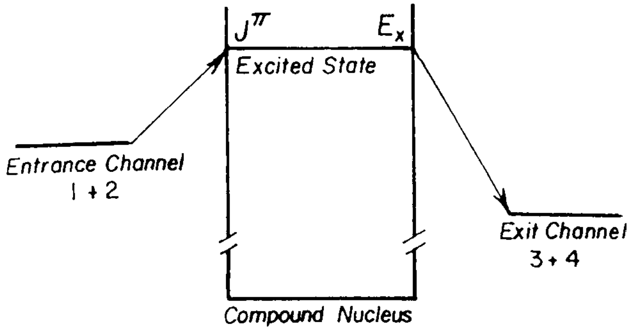

Fig. 2.6. Schematic of a compound-nucleus reaction.

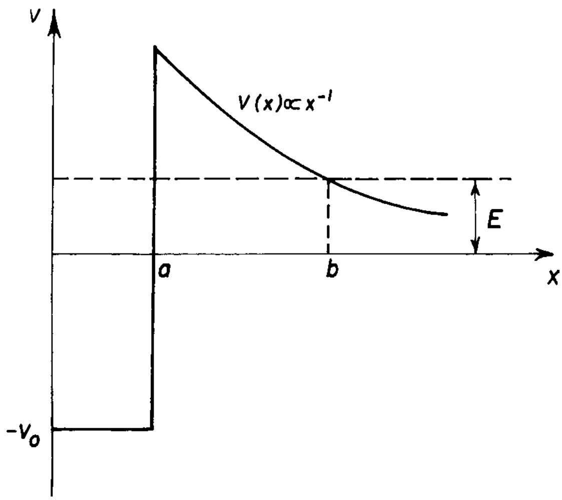

Fig. 2.7. Coulomb barrier penetration by a charged particle. a is the range of the nuclear force and b the classical turning point.

The matrix elements in angle brackets contain nuclear factors and (in the case of charged particles) the Coulomb barrier penetration probabilities or Gamow factors, originally calculated in the theory of α-decay, which can be roughly estimated as follows (Fig. 2.7).

A particle with energy E moving one-dimensionally along the negative x-axis in a potential $V(x)$ is described quantum-mechanically by a plane wave

$$\Psi = A\, e^{i(\omega t + kx)} = A\, e^{\frac{i}{\hbar}(Et + \sqrt{[2m(E-V)]}x)}. \tag{2.16}$$

The probability current is conserved for $E > V$. When penetrating the barrier, $E - V$ becomes negative and $\Psi^*\Psi$ decays as $e^{-(2/\hbar)\sqrt{[2m(V(x)-E)]}\delta x}$ as the particle moves from position $x + \delta x$ to position x. The total probability of barrier penetration (neglecting angular momentum which supplies an additional 'centrifugal' barrier) then includes a factor e^{-G}, where

$$G = \frac{2}{\hbar}\int_a^b \surd[2m(V(x) - E)]\,dx = \frac{2(2mE)^{1/2}}{\hbar}\int_a^b \surd\left(\frac{b}{x} - 1\right)dx \qquad (2.17)$$

and

$$b = \frac{Z_1Z_2e^2}{E} = \frac{2Z_1Z_2e^2}{mv^2} \qquad (2.18)$$

is the classical turning point. The integral can be evaluated by an elementary trigonometric substitution, giving

$$G = \frac{4Z_1Z_2e^2}{\hbar v}[\arccos\surd(a/b) - \surd(a/b)\surd(1 - a/b)]. \qquad (2.19)$$

Since $a \ll b$ (typically by a factor of order 100), the factor in brackets is nearly $\pi/2$ and is quite insensitive to the value of a. Numerically, the barrier penetration probability for s-waves is thus

$$P \propto e^{-2\pi Z_1Z_2e^2/(\hbar v)} \equiv e^{-2\pi\eta} = e^{-BE^{-1/2}} \qquad (2.20)$$

where

$$B = (2m)^{\frac{1}{2}}\pi Z_1Z_2e^2/\hbar = 31.3\, Z_1Z_2A^{\frac{1}{2}}; \qquad (2.21)$$

A is the reduced mass in amu and E is in keV. For example, for 1 keV protons, $P \sim 10^{-9}$, but the penetration probability is enhanced at high densities by electron screening effects. At very high densities, so-called pycnonuclear reactions occur, even at low temperatures, owing to quantum tunnelling and kinetic energy from vibrations in a solid lattice. Pycnonuclear reactions set in quite suddenly above a certain critical density, which (in gm cm^{-3}) is of the order of 10^6 for hydrogen, 10^9 for He and 10^{10} for C; such densities can be reached in accreting white dwarfs and advanced burning stages of massive stars.

The steep dependence of P on energy leads to the use of the 'astrophysical S-factor' defined by

$$\sigma(E) = \frac{1}{E}e^{-2\pi\eta}\,S(E), \qquad (2.22)$$

which contains the purely nuclear part of the cross-section, plus factors of a few in the barrier penetration probability, and varies only slowly with E in the absence of resonances. Laboratory measurements of cross-sections, which usually have to be carried out at higher energies than those mostly relevant in stars, are converted into $S(E)$ to facilitate extrapolation to these lower energies (Fig. 2.8).

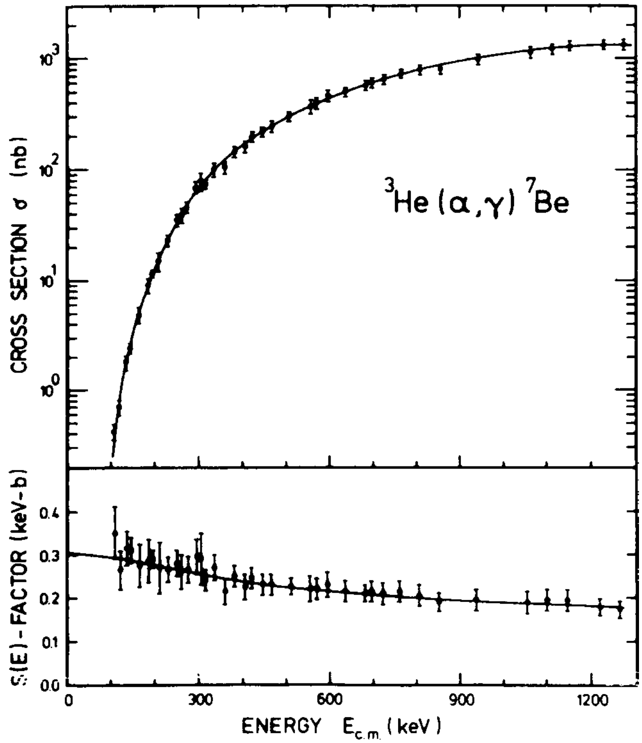

Fig. 2.8. Energy dependence of the cross-section and of $S(E)$ for a typical nuclear reaction. The extrapolation of $S(E)$ to zero energy is carried out with the aid of theory. After Rolfs and Rodney (1988). Copyright by the University of Chicago. Courtesy Claus Rolfs.

A more exact expression for the barrier penetration factor, derived for example by Clayton (1968), is

$$P_\ell(E) = \left(\frac{E_c}{E}\right)^{1/2} \exp\left[-BE^{-1/2} + 4\left(\frac{E_c}{\hbar^2/2mR^2}\right)^{1/2} - 2\left(\ell + \frac{1}{2}\right)^2 \left(\frac{\hbar^2/2mR^2}{E_c}\right)^{1/2}\right] \tag{2.23}$$

or numerically

$$P_\ell(E) = \left(\frac{E_c}{E}\right)^{1/2} \exp[-BE^{-1/2} + 1.05(ARZ_1Z_2)^{1/2} - 7.62\left(\ell + \frac{1}{2}\right)^2 (ARZ_1Z_2)^{-1/2}] \tag{2.24}$$

where

$$E_c = \frac{Z_1Z_2e^2}{R} = 1.0\frac{Z_1Z_2}{A_1^{1/3} + A_2^{1/3}}\ \text{MeV} \tag{2.25}$$

is the height of the Coulomb barrier and R is in fm.

2.4 Sketch of statistical mechanics

Many situations in both nuclear and other parts of astrophysics can be treated to a greater or lesser degree of approximation using concepts of thermodynamic equilibrium. An obvious example is the velocity distribution in classical plasmas, which is Maxwellian to a high degree of approximation under a very wide range of conditions because of the high frequency of elastic collisions, but there are many others. In nuclear reactions at very high temperatures, many reverse reactions proceed with almost the same frequency as forward reactions, leading to a situation of quasi-equilibrium between abundances of the relevant nuclei. Excitation and ionization of atoms, and the dissociation of molecules, follow very precisely thermal equilibrium relations in stellar interiors, and these relations also provide a more or less usable first approximation in stellar atmospheres which is known as local thermodynamic equilibrium. This section therefore gives a brief sketch of relevant parts of statistical thermodynamics, which will have many applications in what follows.

Consider N fermions in a box with fixed energy levels $\tilde{E}_i$ (including rest-mass which itself includes internal excitation energy). To each $\tilde{E}_i$ there correspond ω_i distinct (degenerate) states, made up of g_i internal states and $4\pi V p^2 dp/h^3$ kinetic degrees of freedom, where p is momentum and V is the volume.

Because fermions are indistinguishable and satisfy the Pauli Exclusion Principle, the number of different ways in which each set of ω_i states with energy $\tilde{E}_i$ can have N_i of them occupied is

$$W(N_i, \tilde{E}_i) = \prod_i C_{N_i}^{\omega_i} = \prod_i \frac{\omega_i!}{N_i!\,(\omega_i - N_i)!}. \tag{2.26}$$

Stirling's formula for huge numbers is

$$n! \simeq n^n e^{-n} \tag{2.27}$$

so

$$\ln W = \sum_i [\omega_i \ln \omega_i - N_i \ln N_i - (\omega_i - N_i) \ln(\omega_i - N_i)]. \tag{2.28}$$

Thermal equilibrium implies that, under fixed conditions, W takes on its maximum possible value, i.e.

$$0 = \delta \ln W = \sum_i \delta N_i \, \ln\left(\frac{\omega_i}{N_i} - 1\right) \tag{2.29}$$

subject to overall conditions

$$\sum_i N_i = N, \tag{2.30}$$

the total number (which becomes irrelevant in cases where particles are easily created and destroyed), and

$$\sum_i N_i \tilde{E}_i = \tilde{E}, \tag{2.31}$$

the total energy.

These conditions are incorporated into the stationary condition (2.29) using Lagrange multipliers

$$\sum_i \delta N_i \left[\ln\left(\frac{\omega_i}{N_i} - 1\right) - \alpha - \beta \tilde{E}_i \right] = 0 \quad \forall\, \delta N_i, \tag{2.32}$$

whence

$$N_i = \frac{\omega_i}{e^{\alpha + \beta \tilde{E}_i} + 1}. \tag{2.33}$$

We now appeal to Boltzmann's entropy postulate

$$S = k \ln W \tag{2.34}$$

and let a small reversible change take place. Specifically, we allow some heat and particles to enter a cylinder containing perfect gas at a fixed temperature and pressure. This will lead to a variation in the ω_i's by virtue of the volume change, and

$$\begin{aligned} \delta S &= k \sum_i \delta N_i \,\ln\left(\frac{\omega_i}{N_i} - 1\right) - k \sum_i \delta \omega_i \,\ln\left(1 - \frac{N_i}{\omega_i}\right) \\ &= k(\alpha \delta N + \beta \delta \tilde{E} + \frac{N}{V} \delta V - \cdots). \end{aligned} \tag{2.35}$$

Considering this thought-experiment from the point of view of thermodynamics, the additional particles add enthalpy,

$$dH \equiv d(G + TS) = d\tilde{E} + P dV, \tag{2.36}$$

where G is the Gibbs free energy, i.e.

$$T\, dS \;=\; d\tilde{E} + P dV - \sum_j \mu_j dN_j. \tag{2.37}$$

μ_j is the *chemical potential* of particle species j which is just the specific Gibbs free energy per particle dG/dN_j.[1] Carrying out some divisions in Eq. (2.37),

$$\left(\frac{\partial S}{\partial \tilde{E}}\right)_{V,N_j} = k\beta = \frac{1}{T}; \quad \left(\frac{\partial S}{\partial N_j}\right)_{\tilde{E},V} = k\alpha = -\frac{\mu_j}{T}. \tag{2.38}$$

[1] This case is more rigorously treated in the theory of the 'Grand Canonical Ensemble', which consists of a number of identical systems that are able to exchange heat and particles with a common thermal bath.